Detection and forecasting of shallow landslides: lessons from a natural laboratory

Rupert Bainbridge, Michael Lim, Stuart Dunning, Mike G. Winter, Alejandro Diaz-Moreno, James Martin, Hamdi Torun, Bradley Sparkes, Muhammad W. Khan & Nanlin Jin

Published online: 23 Feb 2022.

Submit your article to this journal ⬀

View related articles ⬀

View Crossmark data ⬀

Detection and forecasting of shallow landslides: lessons from a natural laboratory

Rupert Bainbridge[a] 🆔, Michael Lim[b] 🆔, Stuart Dunning[a] 🆔, Mike G. Winter[c] 🆔, Alejandro Diaz-Moreno[a,d] 🆔, James Martin[b] 🆔, Hamdi Torun[b] 🆔, Bradley Sparkes[e] 🆔, Muhammad W. Khan[b] 🆔 and Nanlin Jin[b] 🆔

[a]Department of Geography, Newcastle University, Newcastle, UK; [b]Faculty of Engineering and Environment, Northumbria University, Newcastle, UK; [c]Winter Associates, Kirknewton, Midlothian, UK; [d]Reynolds International Ltd., Mold, UK; [e]Bridgeway Consulting, Nottingham, UK

ABSTRACT

Rapid shallow landslides are a significant hillslope erosion mechanism and limited understanding of their initiation and development results in persistent risk to infrastructure. Here, we analyse the slope above the strategic A83 Rest and be Thankful road in the west of Scotland. An inventory of 70 landslides (2003–2020) shows three types of shallow landslide, debris flows, creep deformation, and debris falls. Debris flows dominate and account for 5,350 m^3 (98%) of shallow-landslide source volume across the site. We use novel time-lapse vector tracking to detect and quantify slope instabilities, whilst seismometers demonstrate the potential for live detection and location of debris flows. Using on-slope rainfall data, we show that shallow-landslides are typically triggered by abrupt changes in the rainfall trend, characterised by high-intensity, long duration rainstorms, sometimes part of larger seasonal rainfall changes. We derive empirical antecedent precipitation (>62 mm) and intensity-duration (>10 h) thresholds over which shallow-landslides occur. Analysis shows the new thresholds are more effective at raising hazard alerts than the current management plan. The low-cost sensors provide vital notification of increasing hazard, the initiation of movement, and final failure. This approach offers considerable advances to support operational decision-making for infrastructure threatened by complex slope hazards.

1. Introduction

Shallow landslides occur where material fails in the upper layers of a soil profile, usually up to approximately 2 m depth. These landslides usually have little precursory warning and may fail rapidly (e.g., debris flow; Persichillo et al. 2016) or slowly (e.g., creep deformation; Hungr et al. 2014). Their unpredictability means they pose a

significant global hazard, particularly when favourable material and fluidisation conditions transform them into debris flows (e.g., Zimmerman et al. 2020). Debris flows are extremely rapid (>5 m/s), saturated debris-rich landslides that exist along the broad spectrum of flow-like landslides (Hungr et al. 2014). Debris flow runout potential and their capacity to entrain large quantities of water and sediment make them a significant risk where linear infrastructure traverses affected slopes (Geertsema et al. 2009; Meyer et al. 2015). Debris flows can be broadly grouped into channelized debris flows (CDFs) that are constrained for their flow path and hillslope (or open slope) debris flows (HDFs) that occur on non-incised slopes (Chen et al. 2009). CDFs and HDFs can transition into one another where HDFs meet gullies or CDFs breach channels and flow over slopes; it is this hillslope-gully coupling that can control the hazard potential (Milne et al. 2009). CDFs often occur in torrent systems, such as the Illgraben, Switzerland (Badoux et al. 2009), where the repeated flow path removes some of the spatial risk uncertainty and allows focussed monitoring of a single outflow channel.

However, at some sites historic evidence shows debris flows may occur from anywhere across wide areas with suitable topography and materials. This leads to both spatial and temporal uncertainty on triggering location and runout. At such sites, where the risk is high, a combination of active mitigation (physically controlling site aspects using barrier, net, pit, or deflection engineering infrastructure) and passive mitigation (reducing impacts via land-use planning, closures, and warning systems) methods can be used (Huebl and Fiebiger 2005; Vagnon 2020) but can be costly given the wide area of potential source and runout zones. In Scotland, debris flows have repeatedly damaged roads and rail lines resulting in economic and social costs (Winter, Peeling, et al. 2019), with many valleys showing historic (and prehistoric) evidence of multiple debris flow deposits slope wide (Innes 1983; Luckman 1992; Curry 2000). Contemporary infrastructure damaging debris flows have often been linked to high-intensity rainfall (Winter, Ognissanto, et al. 2019). Climate forecasts suggest that in the future Scotland may receive more high intensity rainfall events in the winter and lower-frequency but higher-intensity rainfall during summer months (Jones et al. 2013; UKCP 2018; Finlayson 2020). Such changes in antecedent conditions and rainfall patterns may perturb hillslope sediment cascades (Bennett et al. 2014), releasing sediment from storage that is considered dormant, increasing the rapid shallow landslide hazard in mountainous areas (Winter and Shearer 2017)

Monitoring strategies for determining the level of landslide hazard posed by rainfall, in a given area or slope, vary from global to hyper-local in scale. Global determination of landslide hazard requires the combination of variables such as slope, lithology, soil wetness, antecedent rainfall, and rainfall (Stanley et al. 2021). Whilst useful for global and regional indications of landslide hazard, these global models do not allow detailed analysis of areas smaller than the resolution of the data. Input data are at coarse resolution which do not always accurately represent the real-world spatial variability (Ozturk et al. 2021), making predictions noisy or imprecise. Where a higher confidence in the level of landslide hazard is required for decision making, at linear infrastructure for example, hyper-local monitoring can be deployed. Hyper-local monitoring collects the detail required to make site specific thresholds for
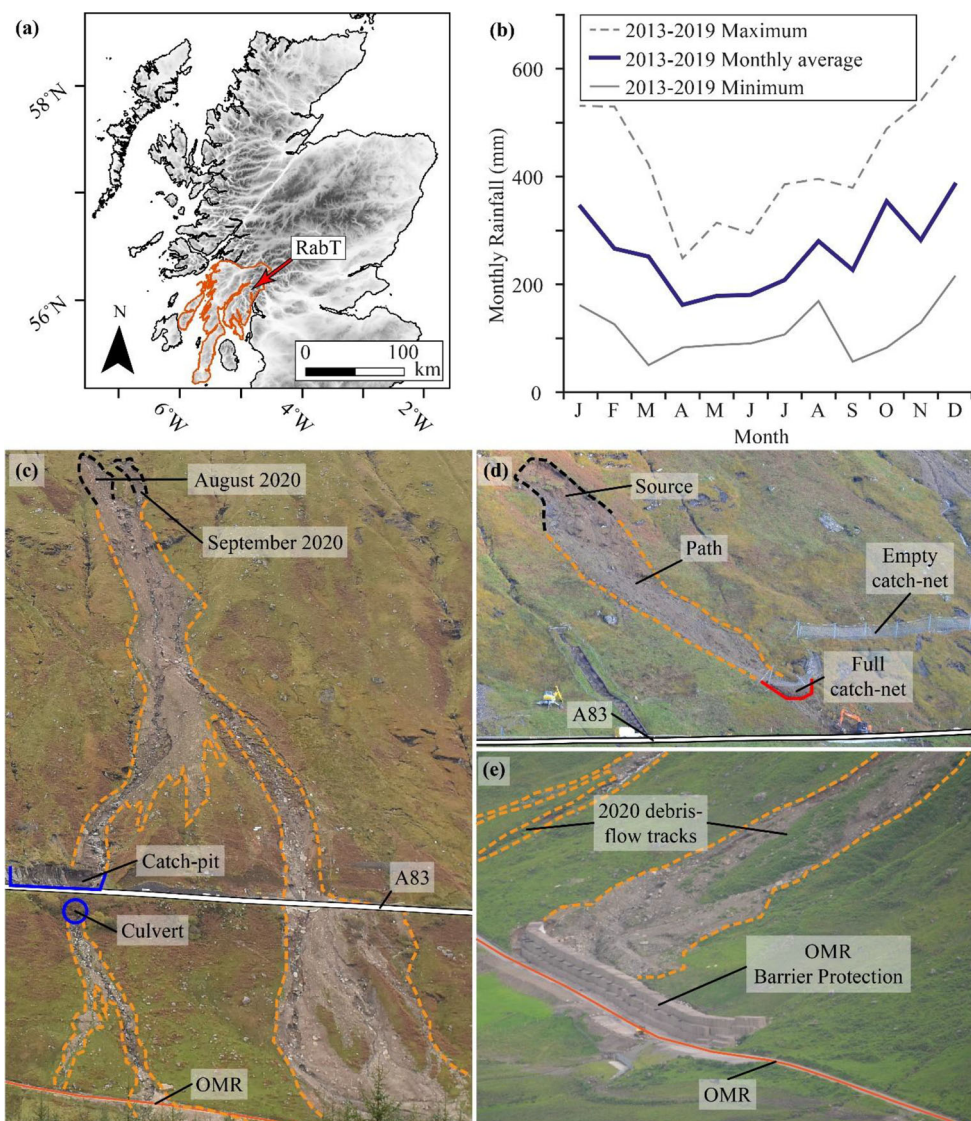
Figure 1. (a) Scotland digital terrain model showing the RabT location (red arrow). The vulnerability shadow (extent of socio-economic impacts) for simultaneous A83/OMR road closures is outlined in orange (modified from Winter, Peeling, et al. 2019). (b) RabT average monthly rainfall from 2013 to 2019 (SEPA RabT gauge; SEPA 2020). (c) Debris flows from August and September 2020 with catch-pit and culvert mitigation. (d) October 9, 2018 debris flow which closed the A83. The catch-net has caught the debris, but some has exceeded the net capacity. (e) View of the OMR debris-flow protection barrier completed in January 2021.

landslide initiation and makes significant improvements over global landslide suscep-tibility models (Ozturk et al. 2021).

Here we demonstrate a novel combination of near-real-time, multi-disciplinary, monitoring techniques that allow remote detection and quantification of slope changes and supplement the regional Landslide Management Plan (LMP). The object-ive of these techniques is to improve our understanding of shallow landslide trigger

mechanisms that threaten road users and infrastructure, and thus enhance alert capabilities for road asset managers at sites that are prone to shallow-landslide/debris flow transitions. These new, relatively low-cost, monitoring techniques and analyses are essential in helping to better manage the present and future increased risk of debris flows.

2. Study area

The A83 Rest and be Thankful (RabT), a key road into and out of west Scotland (Figure 1(a)), bisects the south-western slope of Beinn Luibhean upslope from Glen Croe. This 1.5 km section of road has the highest infrastructure damaging landslide frequency on the Scottish road network (McMillan and Holt 2019). The average slope of the RabT is 32° with a relief of 580 m. The bedrock is Schist, with overlying glacial till up to 3 m thick, interspersed with gullies, landslide source scars, levees and lower slope debris cones (Sparkes et al. 2017, Finlayson 2020, BGS. 2020). The surficial till deposits extend beyond the RabT site and cover much of the lower and mid-slopes of the surrounding hills in the Trossachs mountain range (BGS. 2020) where the A83 and other strategic roads route to the west and north of Scotland.

Average annual rainfall from 2013 to 2019 at the Scottish Environmental Protection Agency (SEPA) Rest and Be Thankful rainfall gauge, located approximately 850 m away from the RabT slope, is 3118 mm per year, with on average most rainfall occurring in October to February (Figure 1(b)). However, August also appears to be generally as wet as winter months and there is considerable variation in monthly rainfall between different years (Figure 1(b)). The RabT is a good proxy for many sediment laden upland/mountainous systems subject to moderate to high rainfall that are susceptible to a range of slope instabilities and threaten infrastructure.

On average 4,000 vehicles cross the RabT per day (Winter, Peeling, et al. 2019). Closures divert traffic a maximum 88 km, if the A83 and Old Military Road (OMR; Figure 1(c)), a one-way convoy diversion downslope of the A83, are closed, casting a vulnerability shadow over 4,300 km^2 (Figure 1(a); Winter, Peeling, et al. 2019). A full road closure costs approximately £90k per day (2012 prices; Winter, Peeling, et al. 2019) and £13.3 M has been spent on active protection of the A83, using catch-nets, catch-pits and culvert upgrades (Figure 1(c,d)). This cost also includes improving the OMR to handle larger vehicles and higher traffic volumes (Scottish Parliament 2020). However, some debris flows still exceed mitigation measures and impact the A83 and OMR. From the August 2020 to January 2021 the A83 was closed for 120 days, due to a series of large debris flows in August and September 2020 (Figure 1(c)). The OMR convoy diversion was in place for much of the closure time, but additional investment was made to build a 175 m long, 6.6 m tall barrier, completed in January 2021 which protects part of the OMR from debris flows (Figure 1(e)). The barrier was installed as a response to the August-September 2020 debris flows and a period of persistent slope creep above the A83 following those events.

The Scottish Road Network Landslide Study examined the full road network landslide risk and mitigation options (Winter et al. 2009). As a result, semi-quantitative and quantitative risk assessments justified additional passive mitigation measures at

the RabT (Winter at al. 2009; Winter and Wong 2020); as part of the LMP daylight patrols are dispatched and warning lights activated on the RabT approach if forecast rainfall is $\geq$25 mm in a 24-hour period or $\geq$4 mm in a 3-hour period (Winter et al. 2020), indicating a raised risk of shallow landslides and therefore debris flows.

3. Datasets and methodology

3.1. Landslide inventories

We have collated a new RabT shallow landslide inventory (available from the Newcastle University Data Repository—https://doi.org/10.25405/data.ncl.c.5308172) from road reports (2003–2015), quarterly and event responsive terrestrial laser scans (TLS; 2015–2020), and time-lapse imagery (2017–2020). Post-2015 it is unlikely events are missing as TLS (0.1 m resolution) and time-lapse imagery data were used (Sparkes et al. 2017; Khan et al. 2021, and this study). Pre-2015, debris flows that reached the A83 are recorded, but other shallow landslides that did not reach the road may not be. The quarterly and event response TLS point cloud data were used to quantify the volume of landslide source areas using the Multiscale Model to Model Cloud Comparison plugin (M3C2; Lague et al. 2013) in Cloud Compare (Version 2.11.3 Anoia; http://www.cloudcompare.org/), which computes distances between two referenced point clouds to show 3-D change. The resulting change data were filtered to extract point-to-point losses and gains due to movement of material on the RabT slope. Longitudinal profiles of CDF and HDF source areas have been extracted from TLS point cloud derived digital elevation models (DEMs) of the RabT slope in QT Modeler (Version 8070, Applied Imagery).

3.2. Rainfall thresholds for landslide alerts

Rainfall on seasonal, daily, and 15-minute timescales are used here as indicators of increased shallow landslide hazard at the RabT. The 2013–2020 seasonal rainfall trend was examined for the Scottish Environment Protection Agency (SEPA) RabT rain gauge data (SEPA 2020) using the Bayesian Estimator of Abrupt change, Seasonality and Trend (BEAST) analysis package (Zhao et al. 2019). BEAST uses ensemble modelling, where multiple competing models analyse data, and Bayesian statistics derive a model average with associated probabilities that detect if seasonal and trend changes are 'true'. BEAST identifies seasonal change points (SCPs) when rainfall has large inter-annual variations, i.e., the seasonal component of the rainfall time-series changes between the same time in different years. Trend change points (TCPs) are identified when the rainfall time-series trend changes abruptly. For seasonal and trend components, not all variations will lead to SCPs and TCPs being assigned, only those that have a high probability of being a genuine and significant difference, based on the agreement between competing models.

September to December 2018 was a particularly active landslide period at the RabT and the start of high-temporal and high-spatial resolution datasets at the site, enabling the association of shallow landslide occurrence to rainfall conditions.

Therefore, this period is used to look in detail at rainfall conditions at and prior to shallow landslide occurrence.

We calculated the Antecedent Precipitation Index (API; Fedora and Beschta 1989), a proxy for ground saturation (Segoni et al. 2018), for daily rainfall totals using Equation 1, as an indicator of raised shallow landslide hazard.

$$API_i = k(API_{i-1}) + P_i \qquad (1)$$

Where API_i is the API at time i, P_i is the daily rainfall total at i and k is a constant decay function defined by the user ($k = 0.8$). The k value is a conservative estimate based on other works (Fedora and Beschta 1989; Viessman and Lewis 1996; Heggen 2001) as no stream gauge data is available for Glen Croe, so storm hydrograph regression analysis to derive a local k estimate was not possible. Rainfall has been measured with an on-slope Davis Vantage Pro 2 gauge (364 m a.s.l) since April 2018, better reflecting on-slope conditions than the off-slope SEPA gauge that is 0.85 km away and 87 m lower in the valley.

Using 15-minute rainfall intensity data from the on-slope Davis Vantage Pro 2 gauge, we developed an intensity-duration (I-D) threshold over which shallow landslides have occurred in the past. Duration and mean rain intensity for all storms in the study period were plotted (Guzzetti et al. 2008; Brunetti et al. 2010), with a six-hour inter-event period. An I-D threshold above which landslides occur was visually derived from the results (Guzzetti et al. 2008). Mean rain intensity over an entire storm was used, as opposed to mean rain intensity up to the point of the landslide, as not all landslide timings were known due to occlusion of the slope from the time lapse camera by clouds and at night-time.

3.3. Landslide initiation, tracking and detection

Remote monitoring to detect slope changes can be useful for assessing slope conditions and managing infrastructure, without needing a constant personnel presence on-site. Visual analysis of imagery is useful, however an ability to analyse images pixel-by-pixel, detect changes, and quantify rates of movement provides more data to asset managers. With this ability large areas can be analysed for precursory movement before landslides occur as well as tracking and detecting movement during slope failures. Here, we process time-lapse imagery in a particle image velocimetry tool (PIVLab; Thielicke and Stamhuis 2014; Thielicke 2020) to detect creeping deformation on the RabT during mid- to late-September 2018, before a series of road-closing debris flows in October 2018. This time-period is used here as a good example of what this technology and these data can achieve prior to a series of large slope failures. This PIV tool has since been enhanced by Khan et al. (2021) for automatic image stabilisation, processing, and filtering. Displacement vectors and velocity were established between consecutive slope-wide images at 16×16 pixel resolution (approximately $2.7 \, m^2$). Sequential deformation was derived for a point tracked through the photo sequence and inverse velocity (I-V), an analytical approach used to predict failure in brittle materials (Carlà et al. 2017), was used as an indicative metric for till failure prediction. Despite the non-brittle materials involved, some

Table 1. Summary of contribution (by area and volume) of different material source areas to the slope failure types occurring at the site.

	Debris cones	Till	Regolith
Number of debris flows and debris falls	11	21	11
Number of creep landslides	7	3	0
% areal slope coverage	22	61	18
% source area volume contribution	18	67	15

shallow landslides at the RabT appear to move as rafts of intact material over a discrete, progressively forming shear surface, and, as such have more in common with brittle failure than ductile deformation. Imminent failure is predicted when I-V values reach zero (infinite velocity), in theory, and, occasionally in practice this time can be derived from monitoring data (Fan et al. 2019; Xu et al. 2020). Intervals between usable daylight images was not uniform due to cloud, rain, and night-time obscuration, so velocity data from PIVLab were interpolated to 12 h intervals, with a moving average smoothing of 24 h. I-V was calculated for smoothed data using $1/(Vw)$ (e.g., Manconi and Giordan 2016), where V is velocity over the defined time window (w).

We used seismic monitoring to detect the precise timing of the onset of a shallow landslide that transitioned to a debris flow. Industry standard seismometers are used for the detection of debris flows in catchment scale torrent systems (Walter et al. 2017) and the slope failure source areas that cause them (Burtin et al. 2014). Here we deploy a low-cost Raspberry Shake 3D seismometer (Manconi et al. 2018; Raspberry Shake 2020) for directional detection of debris flows on a steep hillslope with uncertain flow initiation and routing, and short flow paths. The seismogram trace shows characteristic debris flow signals (Burtin et al. 2014), generated through clast-clast and flow-substrate interactions, above the long-term average. Conventional seismics uses cross-correlation between stations to geolocate the event generating the seismic signal (Burtin et al. 2014). Here we use hodograms (plotting signal direction through time; Borella et al. 2019) to confirm the direction of debris flow signals to the seismometer as we only had a single station deployed on the site.

4. Results

Effective road asset management requires information on raised threats of landslide activity, significant slope changes, precursory movement and, finally, post-failure adjustment during remedial works. These data all need the context of long-term activity. This enables stakeholders to be on stand-by, pre-position resources, or pro-actively manage risk with targeted interventions. Here we show how the methodologies are applied to achieve alerts of high activity periods within long-term records, to quantify threshold preconditions to failure, and to create 'event happened' warnings that have been integrated into the management of the RabT.

4.1. Long-term landslide activity

From 2003 to 2020 there were 70 shallow landslides which presented as three different landslide types: 49 were debris flows (21 HDFs, 25 CDFs, three of unknown
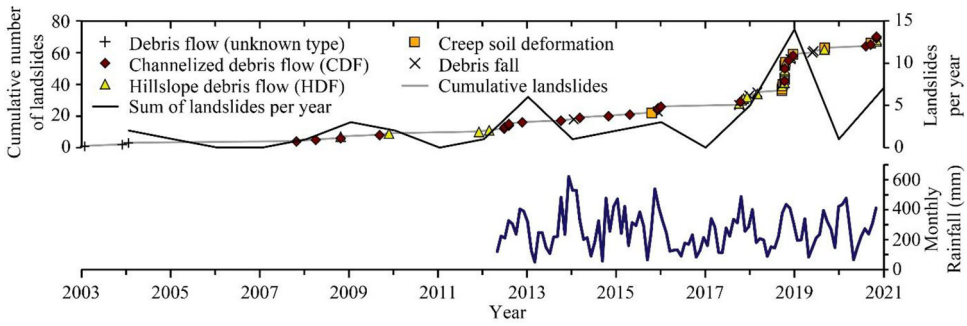
Figure 2. 2003 to 2020 cumulative landslide timeseries and yearly totals. Monthly rainfall is shown from the off-slope SEPA Rest and be Thankful gauge from 2012 to 2020 (no rainfall gauges were installed in the vicinity of the slope pre-2012, therefore no rainfall data is available before this time).
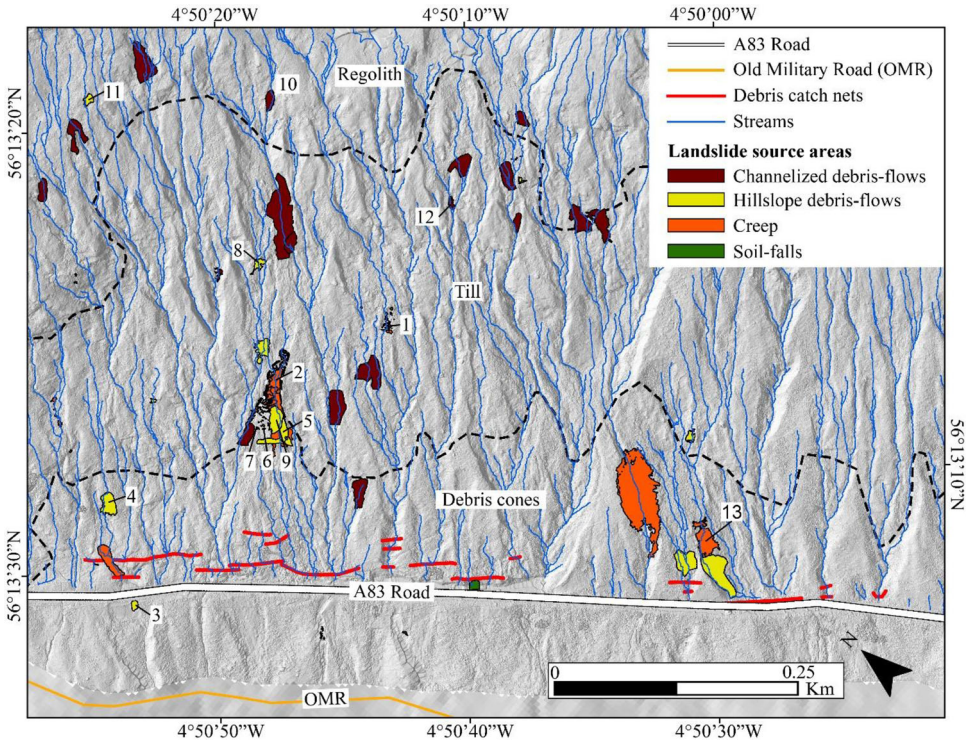
Figure 3. RabT landslide inventory. TLS derived hillshade and 2007 to 2020 landslide source areas, coloured by the resulting failure type. Surface material delineation (dashed lines) modified from Finlayson 2020. Numbers refer to Figure 6.

type); 12 slope creep events, defined as a relatively slow gravitational deformation of material; and 9 debris falls (Hungr et al. 2014); Debris falls in the literature are defined as a "detachment, fall, rolling and bouncing of soil fragments … or blocks of cohesive soil" (Hungr et al., p.169 Table 1, and p.172 Section 2), which in the case of the RabT are small, approximately $1 \, m^3$, failures of surficial material, often from the

**Table 2.** Descriptive statistics for the depth profiles in Figure 4.

	Inventory landslide number					
	41	47	48	49	50	51
Material	Debris	Debris	Till	Debris	Regolith	Debris
Minimum depth	0.03	0.63	0.21	0.47	0.13	0.34
Maximum depth	2.3	7.6	1.61	1.79	1.75	3.27
Average depth	0.79	3.33	0.94	0.85	0.83	1.54
Standard deviation of profile depth	0.62	1.82	0.43	0.32	0.34	0.7

	Inventory landslide number					
	53	55	57	58	64	65
Material	Regolith	Regolith	Till	Till	Till	Till
Minimum depth	0.08	0.32	0.53	0.2	0.27	0.04
Maximum depth	1.27	1.22	0.72	1.93	2.6	3.2
Average depth	0.64	0.81	0.4	1.02	1.54	2.15
Standard deviation of profile depth	0.04	0.24	0.74	0.49	0.61	0.79
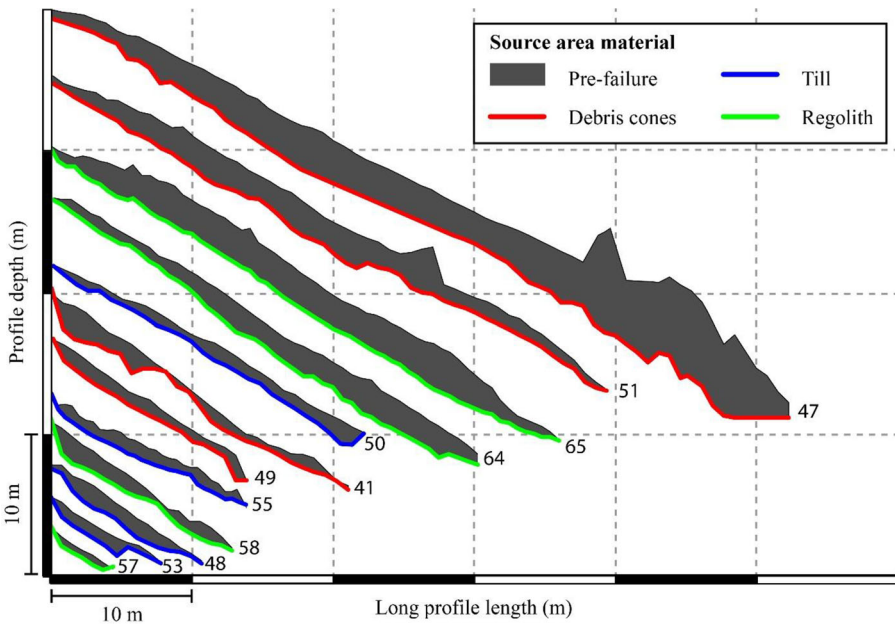
Figure 4. Example debris flow source area long profiles (2018–2020), derived from TLS point clouds, showing pre- and post-failure surface elevations. Profiles are coloured by source material type. Profiles are numbered by the landslide inventory.
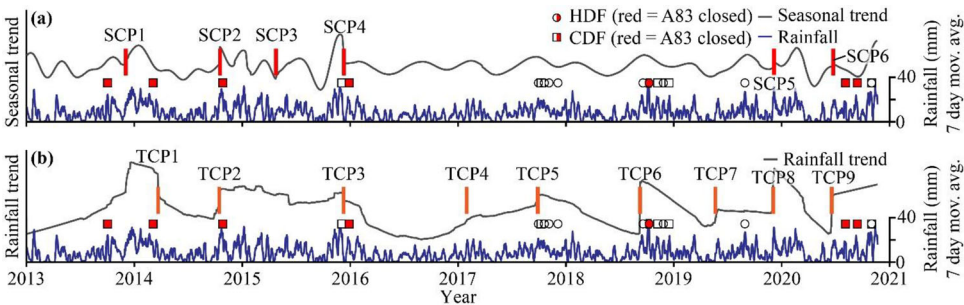
Figure 5. (a) BEAST seasonal rainfall component. (b) BEAST rainfall trend.
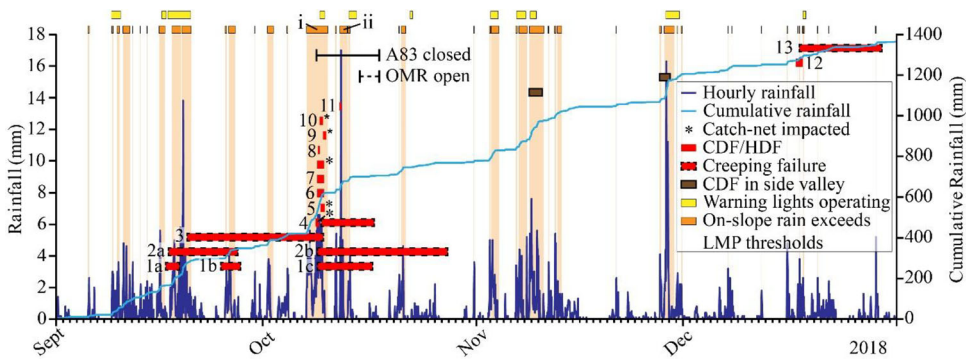
Figure 6. 01 September to 31 December 2018 landslides, warning light activations from the current LMP thresholds (where forecast data is used) and activations that would have occurred using real-time on-slope data. On-slope rainfall data is from the Newcastle University Davis gauge.

top of bedrock outcrops, which do not propagate far downslope (Figure 2). Seventeen debris flows closed the A83, on average once a year since 2003 though this masks the often clustered nature of events in time; eight reached the OMR which requires a full diversion.

Sixty-three of the landslides have known source locations (Figure 3), 46% (n = 29) are in till, 35% (n = 22) in debris cones and 19% (n = 12) in regolith; 53 have volumetric information derived from TLS (2015–2020) or estimates from reports (2007–2015). Thirty-six are debris flows, seven debris falls and ten creep deformations. Combining the debris flows and debris falls, 18% of the landslide source volume originates from the debris cones (22% of the slope by area); whilst till (61% of the slope by area) and regolith (18% of the slope by area) account for 67% and 15% of the landslide source volume respectively (Table 1). Creep landslide volumes were excluded from the above volumetric analysis, as it is not possible to accurately measure the volume of the entire moving mass from TLS data, given that much of the failed material has not been evacuated from the source area. For creep landslides it is only possible to calculate the surface volume loss. Creep landslides were found in the debris cones (n = 7) and till (n = 3). Most of the surface volume loss from creep deformation occurred in the debris cones (5,673 m^3) and very little within the till (26 m^3) despite its larger coverage over the slope (Figure 3).

Volumetric contributions from different materials reflect distinct failure processes and physical controls such as depth to bedrock. Failures originating from debris cone source areas are generally long (15–50 m) and have the deepest recorded failures; there is a more varied original surface-to-failure plane depth profile from debris-cone sources (Table 2; Figure 4). Till-based failure planes vary between 5 m and 35 m in length with a shallower depth profile (average 1.2 m); whilst regolith failures are between 5 m to 25 m with a shallow average depth profile of 0.77 m (Figure 4). The average surface slope of the RabT is 32° and average failure plane slopes for all material types range between 30° and 31°. Extrapolation of gully pathways from a

Table 3. Warning light and on-slope alert operation confusion matrix.

% of study period	Landslide	No landslide
Warning lights ON / On-Slope ON	6.6% / 7.7%	4.1% / 11.1%
Warning lights OFF / On-Slope OFF	2.8% / 1.1%	86.5% / 80.1%
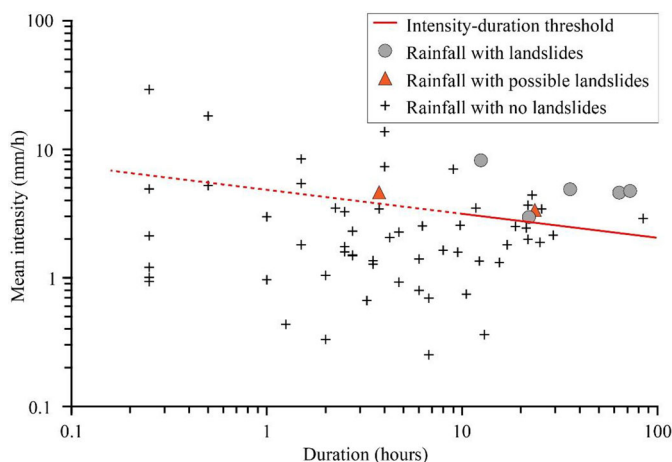
Figure 7. September to December rainstorm intensity-duration (I-D) plot. The solid red line is the intensity-duration threshold above 10 hours duration. Below 10 h duration the threshold is a dashed red line as there was no input data for <10 h landslide inducing rainstorms, this is an extrapolation.

TLS derived DEM, shows a strong coupling of source areas with stream flow paths (streams in Figure 3).

## 4.2. The likelihood of failure: rainfall thresholds

Rainfall on seasonal, daily, and 15-minute timescales has been used to indicate raised landslide hazard. BEAST identified six rainfall seasonal change points (SCP) in winter periods from 2013 to 2020 (Figure 5(a)). SCP4 coincides with Storms Desmond and Frank which caused debris flows at the RabT. SCP6 in mid-2020 shortly precedes the large August-September debris flows that shut the A83. No SCPs are seen from 2016 to late-2019, but debris flows do still occur. Instead, many debris flows are coincident with abrupt rainfall trend change points (TCPs) as well as their subsequent falling trends, and long period high trends (Figure 5(b)). TCPs 1, 2, 3, 5, 6 and 9 are all associated with debris flow occurrence.

TCP6 starts the 2018 landslide period, a particularly active year with 19 of the 63 shallow landslides (Figure 2). Here we use September to December 2018, a particularly active time-period at the RabT, as a case study to highlight the effectiveness of pro-active, near-real-time monitoring to alert asset managers to increased shallow landslide hazard based on rainfall thresholds, tracking slope creep, and detecting debris flow occurrence. Time-lapse imagery has allowed the timings of the 2018 landslides to be more accurately detected, allowing the identification of specific rainstorms where landslides have occurred.

Table 4. API and I-D threshold confusion matrix. Current LMP statistics are summarised in Table 3.

% of study period	Landslide	No landslide
API > threshold / I-D > threshold	29.5% / 8.2%	0.8% / 5.7%
API < threshold / I-D < threshold	3.3% / 0.0%	81.0% / 86.1%
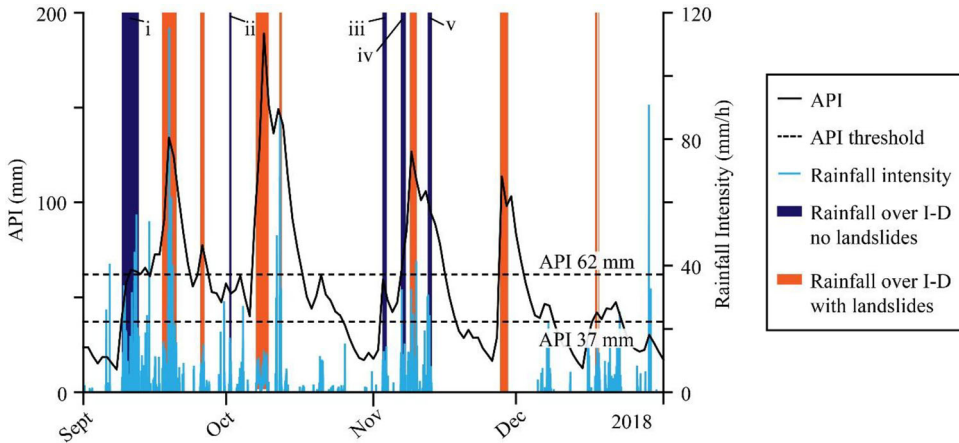
Figure 8. Antecedent Precipitation Index (API) with 37 mm and 62 mm thresholds. Rainfall intensity (data loss 13 November to 05 December) with storms >10 h duration exceeding the I-D threshold.

For the late-2018 period Figure 6 shows when LMP forecast rainfall thresholds were exceeded and warning lights were operating, along with the same thresholds plotted using on-slope, live rain data. These data are summarized in confusion matrices which describe the performance of the rainfall thresholds in detecting conditions that triggered shallow landslides; data are described as times where thresholds predict landslides will or will not happen against times where landslides did or did not occur. False alarms and missed landslides account for 6.9% of the study period for warning lights and 12.2% for on-slope data (Table 3).

Warning lights are human operated, reducing false alarms through expert judgement. However, on-slope data would raise alert levels two times where shallow landslides (particularly debris flows) occurred, that are not fully covered by the warning lights (Figure 6(i, ii)). To improve on the current LMP rainfall thresholds for predicting hazardous shallow landslide conditions on the RabT, shown in Table 3 and Figure 6, we now look at the intensity and duration of rainstorms which generated landslides, and antecedent precipitation.

Landslide producing storms in 2018 were medium (>10 h) to long duration (max. 72 h; Figure 7); however, for two storms it was not possible to determine in which the landslide happened. Mean rain intensity for landslide initiation ranges from 2.95 mm/hr to 8.15 mm/hr. Landslides occur above the threshold described by Equation 2.

$$I = 4.75D^{-0.18} \tag{2}$$

Where I is mean rain intensity and D is duration. All confirmed landslide storms were >10 h duration, so it is unclear if the threshold applies to storms of <10 h
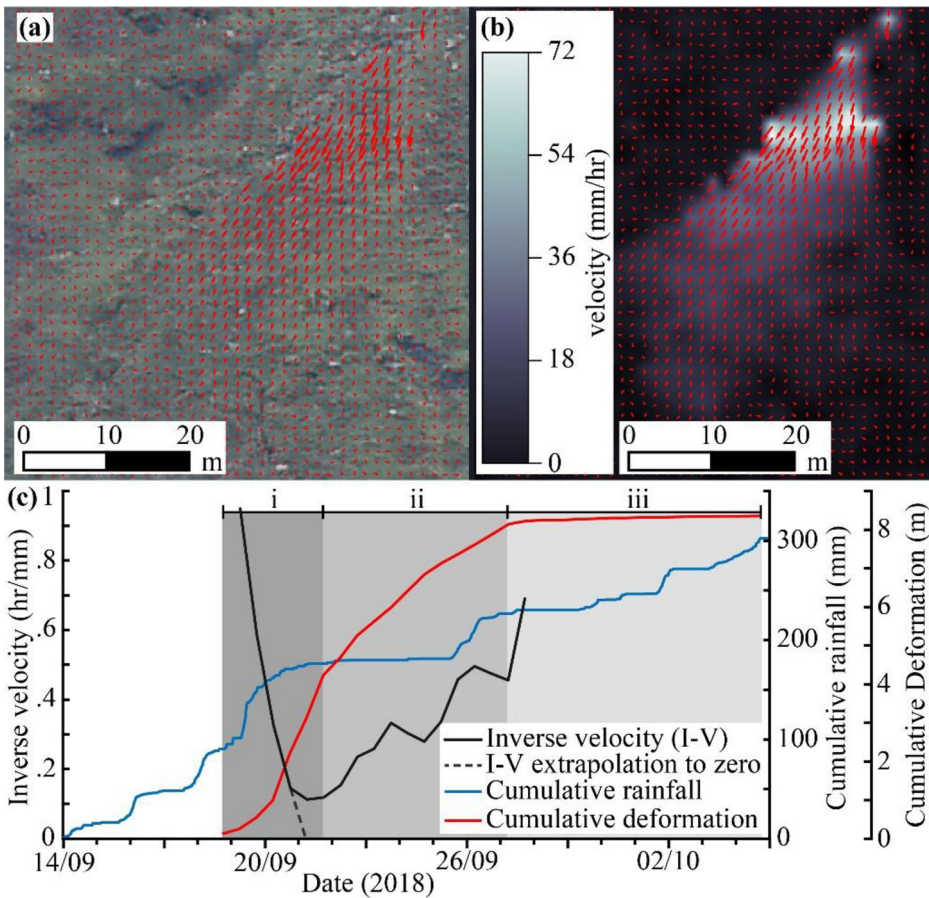
Figure 9. (a) PIVLab deformation vector plot (Thielicke and Stamhuis 2014). (b) Velocity heat map. (c) Cumulative rainfall, cumulative deformation, and I-V.

duration. The threshold has been extrapolated for storms under 10 h duration but dashed on Figure 7 to show its uncertainty. The I-D threshold gives a false alarm for 5.7% of the study period (Table 4).

All landslides (n = 18) occur over an API threshold of 37 mm, with three false alarms and long periods of alert with no landslides (Figure 8). A 62 mm API threshold covers 90% of landslides (n = 16), reduces false alarms to 0.8% of the study period (Table 4), but misses two mid-December events. A combination of I-D and API thresholds maximizes landslide detection and minimizes false alarms (Table 4). All landslide inducing storms exceed the I-D threshold with five false alarms (Figure 8(i–v)) which API thresholds reduce to two (Figure 8(iv, v)).

4.3. Early warning of slow creeping failures

We monitored the creep of Failure 2 (Figure 6) via time-lapse image vector tracking from initiation (19 September 2018) to arrest (27 September 2018) using PIVLab
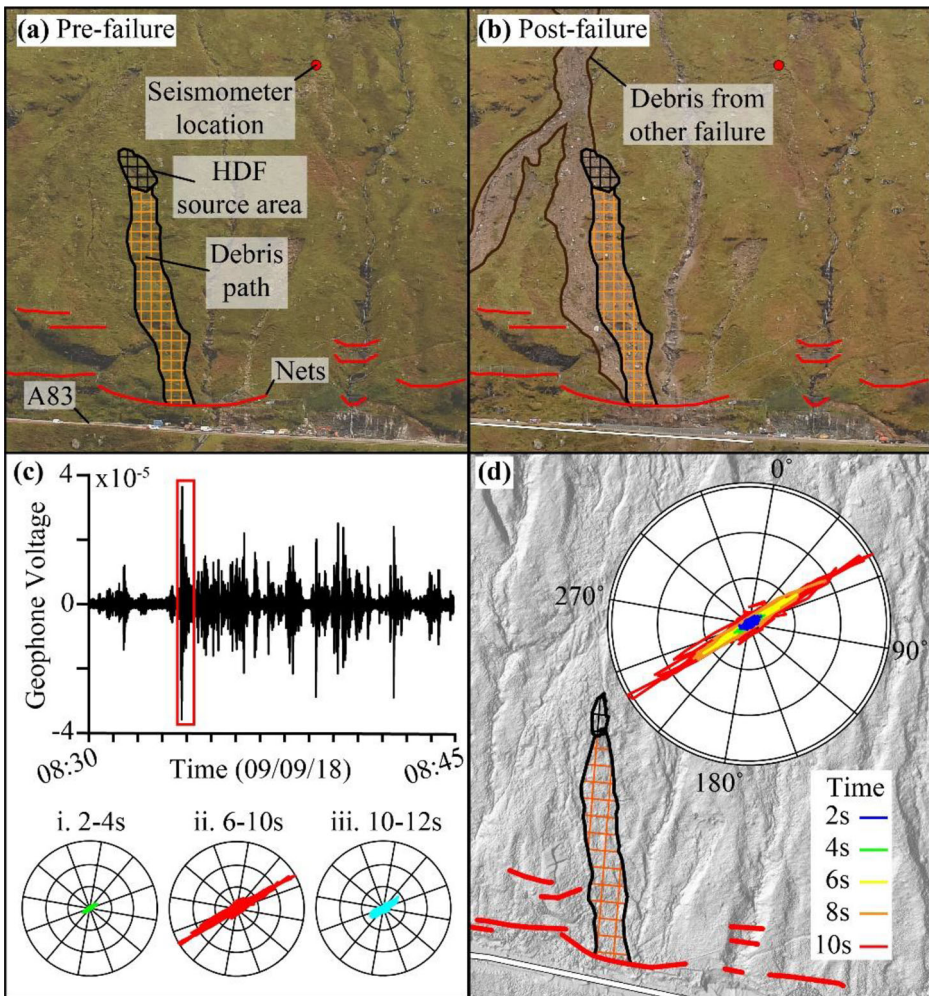
Figure 10. (a) Pre-failure HDF source and seismometer location. (b) Post-failure. (c) Fifteen-minute seismogram with HDF signal (red box) and three hodogram time-steps (i, ii, iii). (d) Hillshade with HDF location and ten second stacked hodogram.

(Thielicke and Stamhuis 2014; Thielicke 2020; Khan et al. 2021). Vectors of change and a velocity heat map between consecutive images are shown in Figure 9(a,b).

Creep initiation coincides with a rainstorm on the 18 September 2018 (Figure 9(c), i). Half of the total cumulative deformation occurs in the first 2.5 days. Inverse velocity (I-V) rapidly decreases towards zero on the 19–20 September 2018; extrapolation of the I-V trend predicts failure on the 21 September 2018. However, I-V values increase on the 21 September, indicating reduced velocity after rainfall ceases. The deformation rate slows until arrest (Figure 9(c), ii) and subsequent rainfall does not affect the deformation rate (Figure 9(c), iii). Operationally, alert levels would be raised in Phase i when imminent failure seemed likely but lowered in Phase ii.

4.4. Detecting rapid debris flows

Seismic monitoring identified a HDF (Figure 10(a,b)) on the 09 October 2018 and located the source area. The z-axis seismogram (Figure 10(c)) shows a high-amplitude signal lasting approximately 15 s, corresponding with the failure time derived from time-lapse imagery, which is likely the HDF in motion. Short duration, lower amplitude signals follow and are likely post-landslide sediment and boulder reworking. Hodograms show very little activity at first (Figure 10(c), i), but signal strength increases as the HDF signal arrives (ii) before subsiding (iii). Stacked hodograms, overlain on a DEM, point to the HDF source area as the direction of the incoming signal (Figure 10(d)).

RabT debris flow seismic signals are brief due to short, steep flow paths, with boulder and sediment reworking post-event. Another deposit on Figure 10(b), which is a thin, fine-grained drape but has a large deposit footprint, was not detected by seismic monitoring; indicating that whilst high debris content flows can be detected, hyper-concentrated flows may need larger station arrays for detection.

5. Discussion

Between 2003 and 2020 there were 70 shallow landslides recorded, including 49 debris flows. Landslides come from three material types on the slope: regolith, till, and debris cones, which exert a control on source area morphology and landslide volumes. Debris cone sources are generally deeper, which likely represents thicker deposits of source material to bedrock. The failure depths sourced in the upslope surface material comprising of glacial till and regolith were significantly shallower. The total volume of source areas for debris flows and debris falls across the slope is 5,404 m^3, with debris cones accounting for 18% (984 m^3), regolith 15% (823 m^3) and till the remaining 67% (3,597 m^3). Each material type accounts for a proportion of source volumes similar to their areal coverage of the slope, indicating that no one material produces relatively more landslide volume than any other. However, debris cones produce fewer but larger landslides, whilst till and regolith sources produce smaller but more frequent landslides. Debris flows in till have closed the road seven times compared to four and three times for regolith and debris cones respectively. Debris flows in till could therefore be considered as the greatest risk to road closure. Similar failure plane slope angles of 30° to 31° indicate a control on landslide initiation, which may represent a critical threshold within the slope material or relate to the dip angle of the underlying bedrock – although most shallow landslides at the site are not at the bedrock-cover interface.

BEAST rainfall analysis shows that debris flows are primarily associated with abrupt rainfall trend changes, but that in some cases there is a larger seasonal signal associated with debris flow occurrence. In the 2018 study period, antecedent, and medium- to long-duration, high-intensity rainfall is shown to be an important factor in debris flows initiation. New local API and I-D rainfall thresholds, identify all landslide inducing storms and minimize false alarms, improve on the LMP and provide road authorities time to consider actions. 90% of RabT landslides occurred over a 62 mm API, indicating a critical antecedent rainfall threshold. Rainstorm I-D > 10 h is

key for landslide initiation with largely higher mean rain intensity than non-landslide storms. Whilst the thresholds have been calculated locally at the RabT, the surface geology and the topography of the site are replicated in, and are representative of the surrounding mountain range, indicating that the thresholds potentially apply more regionally although there is not currently a wider, timed inventory of failures.

Time-lapse vector tracking located and quantified creeping deformation in response to rainfall drivers. I-V calculations forecast imminent failure in the initiation phase, however creep slowed when rainfall ceased and arrested despite further rainfall. This method can detect slope movement and indicate times of heightened risk of failure for management authorities.

Continuous passive seismic detection and hodograms were used to identify a HDF. In this instance, and likely others due to short RabT flow paths, the 15 second event duration is too brief for live warnings but allows for uninterrupted event detection and rapid response, outside of time-lapse image capture. Additional seismometers (now deployed) extend the range of detection and allow more traditional geo-location.

It is not yet known whether climate change has had an impact on the generation of landslides on the slope, not least as the period (2003 to 2020) over which detailed records are available is too short for such an assertion to be made. Similarly, it is not known whether rainstorms that have generated landslides have been getting more intense and longer duration on a persistent basis. It is outside of the scope of this manuscript to examine the impact of climate change. No 'relatively' complete landslide inventories (other than this one) exist for the surrounding area, and it is therefore difficult to contextualise this site in respect to increasing landslide frequency. While we cannot yet link increases in landslide frequency, or magnitude, to climate change, observations certainly indicate that the magnitude of events in 2020 was greater than in living memory and that three of the last four years at the RabT have had some of the most frequent landslide events on record.

6. Conclusions

This paper presents the results of on-site monitoring at the RabT, aimed at supplementing the existing regional LMP (Winter et al. 2009). Our novel combination of sensors and processing techniques allows near-real-time monitoring and quantification of rapid shallow landslides as demonstrated at the RabT in the west of Scotland. Results show that local sensor systems improve our understanding of triggers by allowing landslides to be attributed to specific rainstorms and therefore the conditions leading to their initiation are better quantified. Improved rainfall thresholds for periods of likely increased shallow landslide hazard have been developed for the RabT, however the techniques could be readily applied to other sites of interest. Further, we have shown that creep deformation can be detected and then tracked in near-real time, and, that rapid debris flow failures (which may or may not have shown precursory movement) can be detected. Low-cost sensors can be replicated at high- and lower-risk sites where cost-benefit would normally prevent monitoring. Increased high-intensity rainfall due to climate warming is expected in Scotland (UKCP 2018), meaning more infrastructure and assets will have increased debris flow risk. These

combined low-cost monitoring techniques are an essential advancement and now an operationally proven approach for addressing this future risk.

Disclosure statement

No potential conflict of interest was reported by the authors.

ORCID

Rupert Bainbridge 🆔 http://orcid.org/0000-0002-6375-4956
Michael Lim 🆔 http://orcid.org/0000-0002-6507-6773
Stuart Dunning 🆔 http://orcid.org/0000-0002-2310-7367
Mike G. Winter 🆔 http://orcid.org/0000-0003-3148-619X
Alejandro Diaz-Moreno 🆔 http://orcid.org/0000-0003-3288-3728
James Martin 🆔 http://orcid.org/0000-0002-6615-2301
Hamdi Torun 🆔 http://orcid.org/0000-0002-7882-286X
Bradley Sparkes 🆔 http://orcid.org/0000-0002-4034-8437
Muhammad W. Khan 🆔 http://orcid.org/0000-0002-1567-7781
Nanlin Jin 🆔 http://orcid.org/0000-0002-0990-6381

Data availability statement

Datasets for this research are available from the Newcastle University Data Repository (https://doi.org/10.25405/data.ncl.c.5308172).

References

Badoux A, Graf C, Rhyner J, Kuntner R, McArdell BW. 2009. A debris-flow alarm system for the Alpine Illgraben catchment: design and performance. Nat Hazards. 49(3):517–539.

Bennett GL, Molnar P, McArdell BW, Burlando P. 2014. A probabilistic sediment cascade model of sediment transfer in the Illgraben. Water Resour Res. 50(2):1225–1244.

BGS. 2020. Onshore GeoIndex. [accessed June 2020]. https://mapapps2.bgs.ac.uk/geoindex/home.html.

Borella J, Quigley M, Krauss Z, Lincoln K, Attanayake J, Stamp L, Lanman H, Levine S, Hampton S, Gravley D. 2019. Geologic and geomorphic controls on rockfall hazard: how well do past rockfalls predict future distributions? Nat Hazards Earth Syst Sci. 19(10):2249–2280.

Brunetti MT, Peruccacci S, Rossi M, Luciani S, Valigi D, Guzzetti F. 2010. Rainfall thresholds for the possible occurrence of landslides in Italy. Nat Hazards Earth Syst Sci. 10(3):447–458.

Burtin A, Hovius N, McArdell BW, Turowski JM, Vergne J. 2014. Seismic constraints on dynamic links between geomorphic processes and routing of sediment in a steep mountain catchment. Earth Surf Dynam. 2(1):21–33.

Carlà T, Intrieri E, Di Traglia F, Nolesini T, Gigli G, Casagli N. 2017. Guidelines on the use of inverse velocity method as a tool for setting alarm thresholds and forecasting landslides and structure collapses. Landslides. 14(2):517–534.

Chen J-C, Lin C-W, Wang L-C. 2009. Geomorphic characteristics of hillslope and channelized debris flows: a case study in the Shitou Area of Central Taiwan. J Mt Sci. 6(3):266–273.

Curry AM. 2000. Holocene reworking of drift-mantled hillslopes in the Scottish Highlands. J Quaternary Sci. 15(5):529–541.

Fan X, Xu Q, Liu J, Subramanian SS, He C, Zhu X, Zhou L. 2019. Successful early warning and emergency response of a disastrous rockslide in Guizhou province, China. Landslides. 16(12):2445–2457.

Fedora MA, Beschta RL. 1989. Storm runoff simulation using an Antecedent Precipitation Index (API) model. J Hydrol. 112(1–2):121–133.

Finlayson A. 2020. Glacial conditioning and paraglacial sediment reworking in Glen Croe (the Rest and be Thankful), western Scotland. Proceedings of the Geologists' Association. 131(2):138–154.

Geertsema M, Schwab JW, Blais-Stevens A, Sakals ME. 2009. Landslides impacting linear infrastructure in west central British Columbia. Nat Hazards. 48(1):59–72.

Guzzetti F, Peruccacci S, Rossi M, Stark CP. 2008. The rainfall intensity–duration control of shallow landslides and debris flows: an update. Landslides. 5(1):3–17.

Heggen RJ. 2001. Normalized antecedent precipitation index. J Hydrol Eng. 6(5):377–381.

Huebl J, Fiebiger G. 2005. Debris-flow mitigation measures. In Jakob M, Hungr O, editors. Debris-flow hazards and related phenomena. Berlin (Heidelberg): Springer; p. 445–487.

Hungr O, Leroueil S, Picarelli L. 2014. The Varnes classification of landslide types, an update. Landslides. 11(2):167–194.

Innes JL. 1983. Lichenometric dating of debris-flow deposits in the Scottish Highlands. Earth Surf Process Landforms. 8(6):579–588.

Jones MR, Fowler HJ, Kilsby CG, Blenkinsop S. 2013. An assessment of changes in seasonal and annual extreme rainfall in the UK between 1961 and 2009. Int J Climatol. 33(5):1178–1194.

Khan MW, Dunning S, Bainbridge R, Martin J, Diaz-Moreno A, Torun H, Jin N, Woodward J, Lim M. 2021. Low-cost automatic slope monitoring using vector tracking analyses on live-streamed time-lapse imagery. Remote Sensing. 13(5):893.

Lague D, Brodu N, Leroux J. 2013. Accurate 3D comparison of complex topography with terrestrial laser scanner: Application to the Rangitikei canyon (N-Z). ISPRS J Photogramm Remote Sens. 82:10–26.

Luckman BH. 1992. Debris Flows and Snow Avalanche Landforms in the Lairig Ghru, Cairngorm Mountains, Scotland. Geografiska Annaler: Series A, Physical Geography. 74(2–3):109–121.

Manconi A, Coviello V, Galletti M, Seifert R. 2018. Short communication: Monitoring rockfalls with the Raspberry Shake. Earth Surf Dynam. 6(4):1219–1227.

Manconi A, Giordan D. 2016. Landslide failure forecast in near-real-time. Geomatics Nat Hazards Risk. 7(2):639–648.

Meyer N, Schwanghart W, Korup O, Nadim F. 2015. Roads at risk: traffic detours from debris flows in southern Norway. Nat Hazards Earth Syst Sci. 15(5):985–995.

McMillan FN, Holt CA. 2019. BEAR Scotland NW trunk road maintenance: efficient management of geotechnical emergencies. Q J Eng Geol Hydrogeol. 52(3):286–294.

Milne FD, Werritty A, Davies MCR, Brown MJ. 2009. A recent debris flow event and implications for hazard Management. Q J Eng Geol Hydrogeol. 42(1):51–60.

Ozturk U, Saito H, Matsushi Y, Crisologo I, Schwanghart W. 2021. Can global rainfall estimates (satellite and reanalysis) aid landslide hindcasting? Landslides. 18(9):3119–3133.

Persichillo MG, Bordoni M, Meisina C, Bartelletti C, Barsanti M, Giannecchini R, Avanzi GD, Galanti Y, Cevasco A, Brandolini P, et al. 2016. Shallow landslides susceptibility assessment in different environments. Geomatics, Natural Hazards and Risk. 8(2):748–771.

Raspberry Shake. 2020. [accessed June. 2020]. https://raspberryshake.org/.

Scottish Parliament. 2020. Official Report of the Public Petitions Committee, 5 March 2020. [accessed, July 2020]. http://www.parliament.scot/parliamentarybusiness/report.aspx?r=12561.

Segoni S, Rosi A, Lagomarsino D, Fanti R, Casagli N. 2018. Brief communication: Using averaged soil moisture estimates to improve the performances of a regional-scale landslide early warning system. Nat Hazards Earth Syst Sci. 18(3):807–812.

SEPA 2020. Rest and Be Thankful 15-minute rainfall record. [accessed May 2020]. https://www2.sepa.org.uk/rainfall/.

Sparkes B, Dunning S, Lim M, Winter MG. 2017. Characterisation of recent debris flow activity at the Rest and Be Thankful, Scotland. In: Mikoš, M., Vilímek, V., Yin, Y. and Sassa, K., editors. Advancing Culture of Living with Landslides, Volume 5 Landslides in Different Environments: WLF: Workshop on World Landslide Forum Conference Proceedings; 29 May–2 June 2017; Ljubljana, Slovenia, pp. 51–58.

Stanley TA, Kirschbaum DB, Benz G, Emberson RA, Amatya PM, Medwedeff W, Clark MK. 2021. Data-driven landslide nowcasting at the global scale. Front Earth Sci. 9:640043.

Thielicke W. 2020. PIVlab—particle image velocimetry (PIV) tool. MATLAB Central File Exchange. [accessed July 2020]. https://www.mathworks.com/matlabcentral/fileexchange/27659-pivlab-particle-image-velocimetry-piv-tool.

Thielicke W, Stamhuis EJ. 2014. PIVlab—towards user-friendly, affordable and accurate digital particle image velocimetry in MATLAB. J Open Res Softw. 2(1):e30.

UKCP. 2018. UK climate projections. Met Office. [accessed June 2020]. https://www.metoffice.gov.uk/research/approach/collaboration/ukcp/.

Vagnon F. 2020. Design of active debris flow mitigation measures: a comprehensive analysis of existing impact models. Landslides. 17(2):313–333.

Viessman W, Jr., Lewis GL. 1996. Introduction to hydrology. 4th ed. New York (NY): HarperCollins.

Walter F, Burtin A, McArdell B, Hovius N, Weder B, Turowski JM. 2017. Testing seismic amplitude source location for fast debris-flow detection at Illgraben, Switzerland. Nat Hazards Earth Syst Sci. 17(6):939–955.

Winter MG, Shearer B. 2017. An Extended and Updated Technical Evaluation of Wig-Wag Signs at the A83 Rest and be Thankful. Transport Research Laboratory Published Project Report PPR743. https://trl.co.uk/reports/extended-and-updated-technical-evaluation-wig-wag-signs-a83-rest-and-be-thankful.

Winter MG, Macgregor F, Shackman L. 2009. Scottish road network landslides study: implementation. The Scottish Executive, Edinburgh, UK.

Winter MG, Peeling D, Palmer D, Peeling J. 2019. Economic impacts of landslides and floods on a road network. AUC Geographica. 54(2):207–220.

Winter MG, Ognissanto F, Martin LA. 2019. Rainfall thresholds for landslides deterministic and probabilistic approaches. Transport Research Laboratory Published Project Report PPR901. https://trl.co.uk/reports/rainfall-thresholds-landslides.

Winter MG, Kinnear N, Helman S. 2020. A technical and perceptual evaluation of a novel landslide early warning system. Proceedings, Institution of Civil Engineers (Transport), pp. 1–38.

Winter MG, Wong JCF. 2020. The assessment of quantitative risk to road users from debris flow. Geoenviron Disasters. 7(1):1–19.

Xu Q, Peng D, Zhang S, Zhu X, He C, Qi X, Zhao K, Xiu D, Ju N. 2020. Successful implementations of a real-time and intelligent early warning system for loess landslides on the Heifangtai terrace, China. Eng Geol. 278:105817.

Zhao K, Wulder MA, Hu T, Bright R, Wu Q, Qin H, Li Y, Toman E, Mallick B, Zhang X, et al. 2019. Detecting change-point, trend, and seasonality in satellite time series data to track abrupt changes and nonlinear dynamics: A Bayesian ensemble algorithm. Remote Sens Environ. 232:111181.

Zimmerman F, McArdell BW, Rickli C, Scheidl C. 2020. 2D runout modelling of hillslope debris flows, based on well-documented events in Switzerland. Geosciences. 10(2):70.